

International Journal of Modern Physics E  
 © World Scientific Publishing Company

## Primordial Nucleosynthesis

Alain Coc

*Centre de Sciences Nucléaires et de Sciences de la Matière (CSNSM), CNRS/IN2P3,  
 Univ. Paris-Sud, Université Paris-Saclay, Bâtiment 104, F-91405 Orsay Campus, France  
 coc@csnm.in2p3.fr*

Elisabeth Vangioni

*Institut d'Astrophysique de Paris, UMR-7095 du CNRS, Université Pierre et Marie Curie,  
 98 bis bd Arago, 75014 Paris (France),  
 Sorbonne Universités, Institut Lagrange de Paris, 98 bis bd Arago, 75014 Paris (France)  
 vangioni@iap.fr*

Received October 18, 2021

Revised Day Month Year

Primordial nucleosynthesis, or big bang nucleosynthesis (BBN), is one of the three evidences for the big bang model, together with the expansion of the universe and the Cosmic Microwave Background. There is a good global agreement over a range of nine orders of magnitude between abundances of  $^4\text{He}$ , D,  $^3\text{He}$  and  $^7\text{Li}$  deduced from observations, and calculated in primordial nucleosynthesis. However, there remains a yet-unexplained discrepancy of a factor  $\approx 3$ , between the calculated and observed lithium primordial abundances, that has not been reduced, neither by recent nuclear physics experiments, nor by new observations. The precision in deuterium observations in cosmological clouds has recently improved dramatically, so that nuclear cross sections involved in deuterium BBN need to be known with similar precision. We will shortly discuss nuclear aspects related to BBN of Li and D, BBN with non-standard neutron sources, and finally, improved sensitivity studies using Monte Carlo that can be used in other sites of nucleosynthesis.

*Keywords:* Big Bang Nucleosynthesis; Nuclear reactions; Cosmology.

PACS numbers: 26.35.+c, 98.80.Es, 98.80.Ft

### 1. Introduction

Besides the universal expansion and the cosmic microwave background (CMB) radiation, the third evidence for the hot big-bang model comes from primordial or big bang nucleosynthesis (BBN). During the first  $\approx 20$  minutes of the universe, when it was dense and hot enough for nuclear reactions to take place, BBN produced the so called “light elements”,  $^4\text{He}$ , D,  $^3\text{He}$  and  $^7\text{Li}$ , together with only minute traces of heavier nuclei. There is indeed a good overall agreement between primordial abundances of the light elements either deduced from observations or from primordial nucleosynthesis calculations.

It is worth reminding that *standard* BBN relies on textbook physics and that, with the exception of the baryonic density, all BBN parameters have now been determined by laboratory measurements. However, in the past, BBN has been essential, to first estimate the baryonic density of the universe,  $\rho_B = (1 - 3) \times 10^{-31} \text{ g/cm}^3$ ,<sup>1</sup> and to give an upper limit on the number of neutrino families  $N_\nu \leq 3$ .<sup>2</sup> The number of light neutrino families is now known from the measurement of the  $Z^0$  width by LEP experiments at CERN:  $N_\nu = 2.9840 \pm 0.0082$ .<sup>3</sup> The observations of the anisotropies of CMB by space missions, in particular WMAP<sup>4</sup> and *Planck*,<sup>5,6</sup> have enabled the extraction of cosmological parameters. It includes the baryonic density of the universe which is now measured at better than the percent level, a precision that cannot be matched by BBN. The other quantities that enter into BBN calculations are in the nuclear physics sector and strongly constrained by laboratory experiments. The nuclear reaction rates affecting the production of the  $A < 8$  isotopes have all been measured in nuclear physics laboratories or can be calculated. Hence, there is no more free parameter in standard BBN and the calculated primordial abundances are in principle only affected by the moderate uncertainties in nuclear cross sections. When calculated primordial abundances are compared with astronomical observations in primitive astrophysical sites, agreement is generally good. However, there is a discrepancy for  ${}^7\text{Li}$  that has not yet found a consensual explanation. Besides, the recent improved precision on deuterium observations demands equivalent progress in some nuclear cross sections.

Accordingly, present big bang nucleosynthesis studies are focused on *i*) solving the *lithium problem*, *ii*) improving the accuracy of the predictions to match increasing precision on observations and *iii*) probe the physics of the early universe. Indeed, when we look back in time, it is the ultimate process for which, *a priori*, we know all the physics involved: departure from its predictions could provide hints or constraints on new physics or astrophysics.<sup>7,8</sup>

## 2. Thermal history of the universe

In order to perform the nucleosynthesis calculation one first needs to know the time evolutions of the baryonic density and temperature. They are obtained from the rate of expansion of the universe and thermodynamic considerations. Assuming homogeneity and isotropy, the geometry of the universe is described by the Friedmann–Lemaître–Robertson–Walker metrics:

$$ds^2 = dt^2 - a^2(t) \left( \frac{dr^2}{1 - kr^2} + r^2(d\theta^2 + \sin\theta d\phi^2) \right), \quad (1)$$

where  $a(t)$  is the scale factor, describing the expansion, and  $k = 0$  or  $\pm 1$  marks the absence or sign of space curvature. Using the Einstein equation that links the curvature and energy–momentum tensors leads to the Friedmann equation that links the rate of expansion [ $H(t)$ ] to the energy density:

$$H^2(t) \equiv \left( \frac{\dot{a}}{a} \right)^2 = \frac{8\pi G(\rho_R + \rho_M)}{3} - \frac{k}{a^2} + \frac{\Lambda}{3}, \quad (2)$$

where  $G$  is the gravitational constant,  $\rho_M$  is the non-relativistic matter density,  $\rho_R$  the radiation density and  $\Lambda$  the cosmological constant (see e.g. Weinberg<sup>9</sup>).

When considering the density components of the universe, it is convenient to refer to the *critical density* which corresponds to a flat (i.e. Euclidean) space. It is given by [ $k = 0$ ,  $\Lambda = 0$  in Eq. (2)]:

$$\rho_{0,C} = \frac{3H_0^2}{8\pi G} = 1.88 h^2 \times 10^{-29} \text{ g/cm}^3 \text{ or } 2.9 h^2 \times 10^{11} \text{ M}_\odot/\text{Mpc}^3, \quad (3)$$

where  $H_0 = h \times 100 \text{ km/s/Mpc}$ , is the Hubble constant with  $h \approx 0.68$ .<sup>6</sup> It corresponds to a density of a few hydrogen atoms per cubic meter or one typical galaxy per cubic megaparsec. Densities are usually given relatively to  $\rho_{0,C}$  with the notation  $\Omega \equiv \rho/\rho_{0,C}$ . The total density is very close to the critical density and is dominated by vacuum energy and dark matter contributions while the baryonic matter only amounts to  $\approx 5\%$  of the total density, or 16% of the total matter content. What we can observe with our telescopes, because it emits light, corresponds to only  $\sim 10^{-3}$  of the total density.<sup>10</sup> CMB observations lead to<sup>6a</sup>:

$$\Omega_b \cdot h^2 = 0.02225 \pm 0.00016. \quad (4)$$

Nevertheless, in spite of its modest contribution, baryonic matter is important as this is the only one we know and observe. The corresponding baryonic density, calculated from Eqs. (4) and (3) is  $\rho_B \approx 4 \times 10^{-31} \text{ g/cm}^3$ , only slightly above the first evaluation.<sup>1</sup> It is  $\Omega_b \cdot h^2$  that is used directly in BBN calculations and is provided by CMB analyses, but it is usual to introduce  $\eta$ , the baryon-to-photon number ratio, which remains constant during the expansion (after electron-positron annihilation), and is directly related to the baryonic density relative to the critical density by  $\eta = 2.7377 \times 10^{-8} \Omega_b \cdot h^2$ .<sup>11</sup>

However, at the BBN epoch, the main contributions to the energy density, that govern the expansion rate, are quite different from the present ones. During the expansion, the non-relativistic (dark and baryonic) matter component of the density is diluted according to  $\rho_M \propto a^{-3}$ , while for relativistic particles ("radiation"), there is an additional factor due to redshift and  $\rho_R \propto a^{-4}$ . The two other terms in the right hand side of Eq. 2 scale as  $a^{-2}$  (curvature) and  $a^0$  (cosmological constant  $\Lambda$ ). The important consequence is that during BBN, when  $a$  is  $\approx 10^8$  times smaller than today,  $H(t)$  is only governed by relativistic particles while the baryons, cold dark matter, cosmological constant or curvature terms play no role. Eq. (2) becomes:

$$\frac{1}{a} \frac{da}{dt} = \sqrt{\frac{8\pi G}{3} \frac{g_*(T)}{a_R} \times T^2}, \quad (5)$$

where we have used the Stefan-Boltzmann law  $a_R T^4$  for the radiation energy density. At temperatures slightly above  $10^{10}$  K, the present particles are: photons, electrons, positrons, the three families of neutrinos and antineutrinos plus a few

<sup>a</sup>We consider the constraints obtained with the largest set of data (TT,TE,EE+lowP) without any external data.

neutrons and protons. The effective spin factor,  $g_*$ , decreases whenever the temperature drops below a mass threshold for the particle–antiparticle annihilation of each species. During BBN, only  $e^+$  and  $e^-$  annihilation has to be considered. Hence, the contributions to  $g_*(T)$  (Fig. 1) come from photons, neutrinos and electrons/positrons before they annihilate. The released energy is shared among the other particles they were in equilibrium with: photons and baryons but not neutrinos as it happens after their decoupling (Fig. 1). During the adiabatic expansion

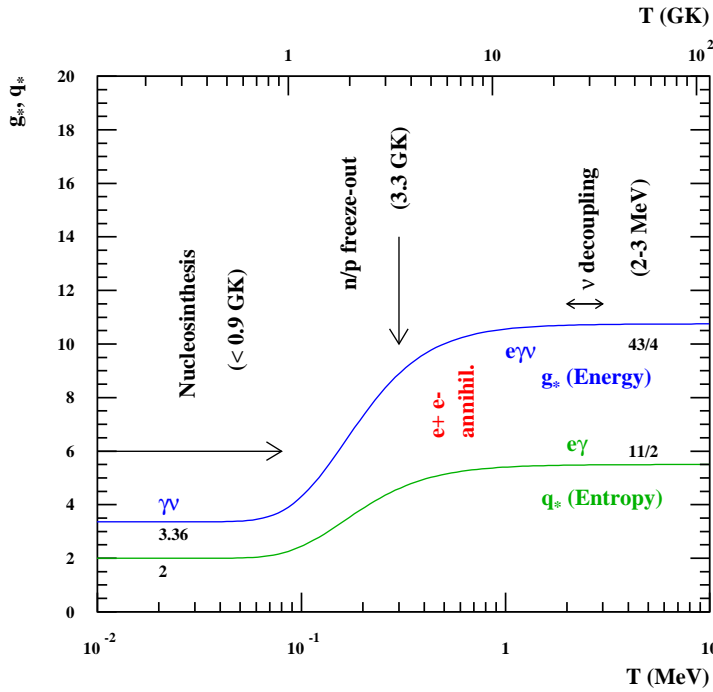


Fig. 1. The spin factors  $g_*$  and  $q_*$  appearing in Eqs. (5) and (7), as a function of temperature, together with the landmarks of BBN.

the entropy densities of neutrinos [Eq. (6)] and photons+electrons [Eq. (7)] stay separately constant:

$$a^3 T_\nu^3 = \text{Cste.} \quad (6)$$

$$a^3 q_*^{e\gamma}(T) T_\gamma^3 = \text{Cste.} \quad (7)$$

with the temperature dependent (due to  $e^+e^-$  annihilation) spin factor,  $q_*$  shown in Fig. 1. Note that the baryonic density does not have at this epoch any influence

on the rate of expansion of the universe (i.e. Hubble parameter). Its influence on nucleosynthesis is simply that a higher density of nuclei induces a larger number of reactions taking place per unit time. Apart from thermonuclear reaction rates, the quantities needed for BBN calculations are the photon/ion temperature  $T(t)$ , the neutrino temperature  $T_\nu(t)$  and the baryonic density  $\rho_B(t) \propto \Omega_b \cdot h^2 a^{-3}(t)$  as a function of time. They are simply obtained by numerically solving Eqs. (5)–(7).<sup>9</sup> Hence, compared to stellar nucleosynthesis, standard big bang nucleosynthesis seems at first as a simple problem without convection, diffusion, or other mixing mechanism, based on known physics, and with most important reactions cross sections measured at the relevant energies. Other differences are that the density during BBN is orders of magnitude lower than in stellar cores, so that three-body reactions (the triple-alpha reaction) are hindered which together with unusual abundances of n, d, t and  ${}^3\text{He}$  lead to different nuclear flows.

### 3. Observed abundances

During the evolution of galaxies, nucleosynthesis takes place mainly in massive stars which release matter enriched in heavy elements into the interstellar medium when they explode as supernovae. Accordingly, the abundance of heavy elements, in star forming gas, increases with time. The observed abundance of *metals* (elements heavier than helium) is hence an indication of age: the older the lower the *metallicity*. Primordial abundances are hence extracted from observations of objects with very small metallicity.

After BBN, concerning the light cosmological elements,  ${}^7\text{Li}$  can be both produced (spallation, AGB stars, novae<sup>b</sup>) and destroyed (in the *interior* of stars). The life expectancy of stars with masses lower than our Sun is larger than the age of the universe so that very old such stars can still be observed in the halo of our Galaxy. In this context, lithium can be observed at the surface of these stars and its abundance was found to be independent of metallicity, below  $\approx 0.1$  of the solar metallicity. This *plateau* was discovered by François and Monique Spite<sup>12</sup> and this constant Li abundance was interpreted as corresponding to the BBN  ${}^7\text{Li}$  production. The thinness of “Spite plateau” is an indication that surface Li depletion may not have been very effective so that it should reflect the primordial value<sup>c</sup>. The analysis of Sbordone et al.<sup>13</sup> gives  $\text{Li}/\text{H} = (1.58 \pm 0.3) \times 10^{-10}$  (i.e. number of atoms relative to hydrogen).

Deuterium is a very fragile isotope. It can only be destroyed after BBN throughout stellar evolution (§ 7). The deuterium abundance closest to primordial abundance is determined from the observation of a few cosmological clouds at high redshift (Fig. 2), on the line of sight of distant quasars. Recently, Cooke et al.<sup>19</sup>

<sup>b</sup>Recent observations<sup>15,16</sup> have confirmed Li production by novae, at a level even higher than model predictions.<sup>17</sup>

<sup>c</sup>Note that recent lithium observations<sup>14</sup> have been done in the Small Magellanic Cloud which has a quarter of the sun’s metallicity and a Li abundance nearly equal to the BBN predictions.

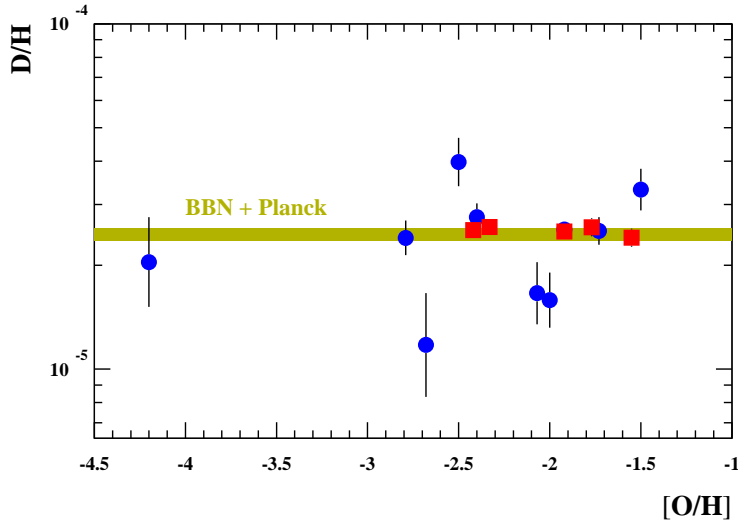


Fig. 2. D/H observations, as a function of metallicity, from Pettini et al.<sup>18</sup> (blue circles) and Cooke et al.<sup>19</sup> (red squares). These most recent observations<sup>19</sup> have very small error bars and show very few dispersion, and are in fair agreement with BBN calculations.<sup>20</sup>

have made new observations and reanalyzed existing data, that lead to a new average value of  $D/H = (2.53 \pm 0.04) \times 10^{-5}$ , lower and with smaller uncertainties than in previous determinations. If such a precision of 1.6% in observations is confirmed, great care should be paid to nuclear cross sections affecting deuterium nucleosynthesis.

After BBN,  ${}^4\text{He}$  is also produced by stars. Its primordial abundance is deduced from observations in HII (ionized hydrogen) regions of compact blue galaxies. Galaxies are thought to be formed by the agglomeration of such dwarf galaxies, in a hierarchical structure formation paradigm, which are hence considered as more primitive. To account for stellar production,  ${}^4\text{He}$  abundance deduced from observations is extrapolated to zero, followed by atomic physics corrections. Aver et al.<sup>21</sup> obtained  $Y_p = 0.2449 \pm 0.0040$  (in mass fraction).

Contrary to  ${}^4\text{He}$ ,  ${}^3\text{He}$  is both produced and destroyed in stars so that the evolution of its abundance as a function of time is not well known. Because of the difficulties of helium observations and the small  ${}^3\text{He}/{}^4\text{He}$  ratio,  ${}^3\text{He}$  has only been observed in our Galaxy:  ${}^3\text{He}/\text{H} = (0.9 - 1.3) \times 10^{-5}$ .<sup>22</sup>

#### 4. Nuclear physics aspects

At high temperature, neutrons and protons are in thermal equilibrium so that, their number ratio is  $N_n/N_p = \exp(-Q_{np}/k_B T)$  where  $Q_{np} = 1.29$  MeV is the neutron-

proton mass difference. This holds until  $T \approx 3.3$  GK, when the weak rates that govern the  $n \leftrightarrow p$  reactions ( $\nu_e + n \leftrightarrow e^- + p$  and  $\bar{\nu}_e + p \leftrightarrow e^+ + n$ ), become slower than the rate of expansion  $H(t)$ . Afterward, the ratio at *freezeout*  $N_n/N_p \approx 0.17$  further decreases to  $N_n/N_p \approx 0.13$  due to free neutron beta decay until the temperature is low enough ( $T \approx 0.9$  GK) for the first nuclear reaction  $n + p \rightarrow D + \gamma$  to become faster than the reverse photodisintegration ( $D + \gamma \rightarrow n + p$ ) that prevented the production of heavier nuclei. From that point on, the remaining neutrons almost entirely end up bound in  ${}^4\text{He}$  while only traces of D,  ${}^3\text{He}$  and  ${}^7\text{Li}$  being produced. Hence, the  ${}^4\text{He}$  yield is directly related to the  $N_n/N_p$  ratio at freezeout that is at the expansion rate  $H(t)$  comparable to the weak rates.

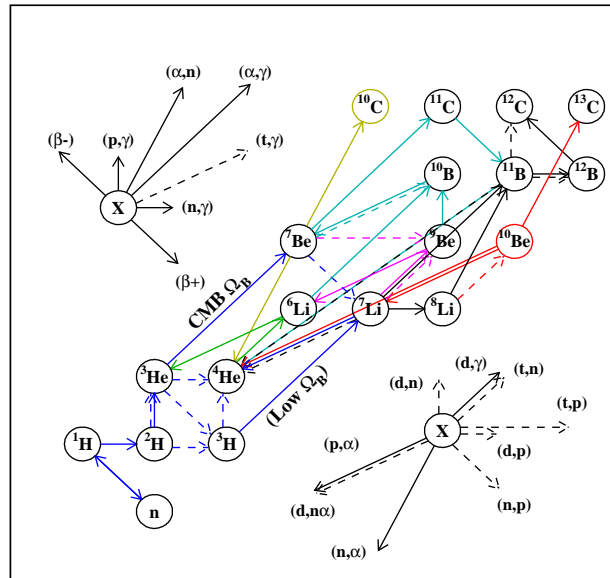


Fig. 3. Nuclear network of the most important reactions in BBN, up to  ${}^7\text{Li}$  (blue), including  ${}^6\text{Li}$  (green),  ${}^{10,11}\text{B}$  (light blue),  ${}^9\text{Be}$  (pink) and up to CNO (black and red). The red arrows represents the newly found reactions that could affect CNO production. The yellow arrows indicate the  ${}^7\text{Be}(d,p)2\alpha$  and  ${}^7\text{Be}+{}^3\text{He}$  reactions that were considered as possible extra  ${}^7\text{Be}$  destruction mechanisms.

Figure 3 displays the most important reactions for the BBN up to CNO, however, only a dozen are important for  ${}^4\text{He}$ , D,  ${}^3\text{He}$  and  ${}^7\text{Li}$  production. There are

many other reactions connecting these isotopes, but their cross sections are too small and/or the reactants too scarce to have any significant effect.

The weak reaction rates, involved in  $n \leftrightarrow p$  equilibrium, come from the standard theory of the weak interaction. They are calculated<sup>23</sup> with, as only experimental input, the neutron lifetime whose experimental value,  $880.3 \pm 1.1$  s,<sup>24</sup> is still a matter of debate<sup>25,26</sup> that affects directly the  ${}^4\text{He}$  production.<sup>27</sup> The  $n+p \rightarrow D+\gamma$  reaction rate<sup>28</sup> is also obtained from theory but in the framework of Effective Field Theory, in good agreement with experiments. For the ten remaining reactions,  ${}^2\text{H}(p,\gamma){}^3\text{He}$ ,  ${}^2\text{H}(d,n){}^3\text{He}$ ,  ${}^2\text{H}(d,p){}^3\text{H}$ ,  ${}^3\text{H}(d,n){}^4\text{He}$ ,  ${}^3\text{H}(\alpha,\gamma){}^7\text{Li}$ ,  ${}^3\text{He}(d,p){}^4\text{He}$ ,  ${}^3\text{He}(n,p){}^3\text{H}$ ,  ${}^3\text{He}(\alpha,\gamma){}^7\text{Be}$ ,  ${}^7\text{Li}(p,\alpha){}^4\text{He}$  and  ${}^7\text{Be}(n,p){}^7\text{Li}$ , cross sections have been measured in the laboratory at the relevant energies (a few 100 keV). This is possible because of the higher energies, hence cross sections, compared to typical stellar nucleosynthesis. Recent compilations of experimental nuclear data to determine thermonuclear rates for BBN, and associated rate uncertainties, were performed by Descouvemont et al.,<sup>29</sup> Cyburt<sup>30</sup> and Serpico et al.<sup>31</sup> for  $A \leq 7$  and by Coc et al.<sup>32</sup> for  $7 < A \leq 12$ .

Since these  $A \leq 7$  evaluations, new experimental data (Di Leva et al.<sup>33</sup> and references therein) has improved the accuracy and reliability of the important reaction  ${}^3\text{He}(\alpha,\gamma){}^7\text{Be}$  rate.<sup>34,35</sup> With the increased precision on deuterium observations, the reactions that govern its nucleosynthesis have also been re-investigated.<sup>20,36</sup> Sensitivity studies (e.g. Ref. 30, 37) have shown that the  ${}^2\text{H}(d,n){}^3\text{He}$ ,  ${}^2\text{H}(d,p){}^3\text{H}$  and  ${}^2\text{H}(p,\gamma){}^3\text{H}$  reactions, are the most influential on D/H predicted abundance. Since the last dedicated BBN evaluations of reaction rates<sup>29–31</sup> a new experiment was performed by Leonard *et al.*<sup>38</sup> They measured both the  ${}^2\text{H}(d,n){}^3\text{He}$ ,  ${}^2\text{H}(d,p){}^3\text{H}$  cross section between  $\approx 50$ – $300$  keV, i.e. well within BBN energy range, with a quoted uncertainty of  $2\% \pm 1\%$ . On the contrary, no new experiment concerning the  ${}^2\text{H}(p,\gamma){}^3\text{H}$  reaction has been conducted so that its rate uncertainty ( $5\%$ – $8\%$ <sup>29</sup>), according to Di Valentino et al.,<sup>36</sup> now dominates the error budget on D/H predictions. For instance, a global increase by an  $\approx 1.10 \pm 0.07$  factor was proposed by Di Valentino et al.<sup>36</sup> and the *Planck* collaboration<sup>6</sup> to better match the CMB and D/H observations. More recently, the  $D(p,\gamma){}^3\text{He}$ ,  $D(d,n){}^3\text{He}$  and  $D(d,p){}^3\text{H}$  experimental data have been used to normalize theoretical  $S$ -factors<sup>39,40</sup> instead of polynomial<sup>30</sup> or R-Matrix<sup>29</sup> fits. For instance Fig. 4 display available experimental  $S$ -factors for the  $D(p,\gamma){}^3\text{He}$  reaction divided by the theoretical prediction from Marcucci et al.<sup>40</sup> after normalization (a factor of 0.99) on the data. The ratio between the previous fits<sup>29,30</sup> with respect to theory<sup>40</sup> show that they are strongly affected by the few experimental data available at BBN energies. By using the normalized theoretical  $S$ -factor instead of fits, the  $D(p,\gamma){}^3\text{He}$  rate is found to be higher at BBN temperatures. Together with a similar treatment for the  $D(d,n){}^3\text{He}$  and  $D(d,p){}^3\text{H}$  data, the D production is naturally reduced (§ 5).

Our BBN calculations take advantage of an extended nuclear network<sup>32</sup> including  $n$ ,  $d$ ,  $t$ ,  ${}^3\text{He}$  and  $\alpha$  induced reactions on targets nuclei up to the CNO region, in order to obtain abundances of  ${}^6\text{Li}$ ,  ${}^9\text{Be}$ ,  ${}^{11}\text{B}$  and CNO isotopes, and to take into account sub-leading nuclear flows that may affect  ${}^4\text{He}$ , D,  ${}^3\text{He}$  and  ${}^7\text{Li}$  abundances.



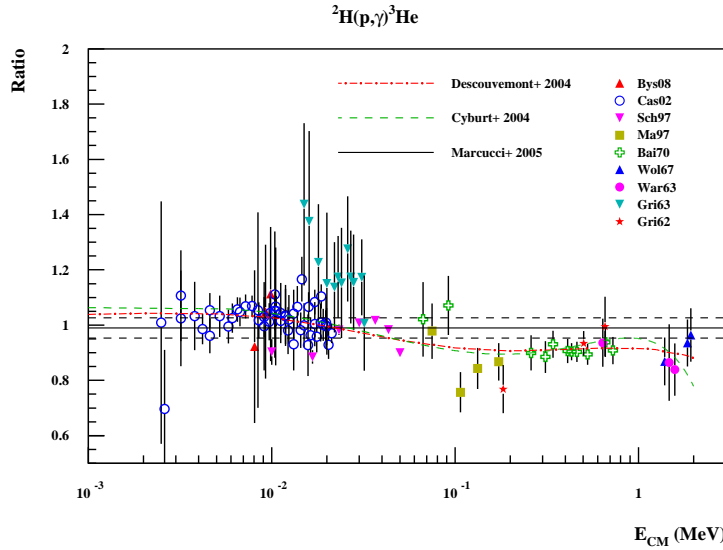


Fig. 4. Ratio of experimental  $S$ -factors to the theoretical one,<sup>40</sup> itself normalized to a subset of the experimental data.<sup>20</sup> Ratio of previous fits<sup>29,30</sup> are driven below theory by the scarce data at BBN energies.

Reaction rates and associated uncertainties, derived from experimental data or from theory (see Ref. 32), are used as input for Monte Carlo BBN calculations to evaluate uncertainties on the resulting abundances and investigate their possible hidden interrelationship with peculiar reactions (§ 8).

## 5. BBN primordial abundances compared to observations

In Figure 5 is represented an updated calculation of the abundances of  $^4\text{He}$ , D,  $^3\text{He}$  and  $^7\text{Li}$ , as a function of the baryonic density where the thickness of the curves reflect the nuclear rate uncertainties. They were obtained by a Monte-Carlo calculation using the nuclear rate uncertainties from Refs. 28, 29, 32, 35, 41. The horizontal areas represent the primordial abundances deduced from observations as discussed above (§ 3). The vertical stripe represents the baryonic density deduced from CMB observations.<sup>6</sup> The calculated primordial abundances at Planck baryonic density are given in Table 1. We can observe small evolutions with respect to earlier works;<sup>11</sup> this comes from slight evolution of the baryonic density and the neutron lifetime but more effectively from updated reaction rates:  $^3\text{He}(\alpha, \gamma)^7\text{Be}$ ,<sup>35</sup>  $\text{D}(\text{p}, \gamma)^3\text{He}$ ,  $\text{D}(\text{d}, \text{n})^3\text{He}$  and  $\text{D}(\text{d}, \text{p})^3\text{H}$ <sup>20</sup> and  $^7\text{Be}(\text{n}, \alpha)^4\text{He}$ .<sup>41</sup> A noticeable change is observed on D/H which is significantly reduced due to the re-evaluation of the three above mentioned reaction rates. As shown on Figure 5 and Table 1, the primordial abundances deduced either by BBN at CMB deduced baryonic density, or from

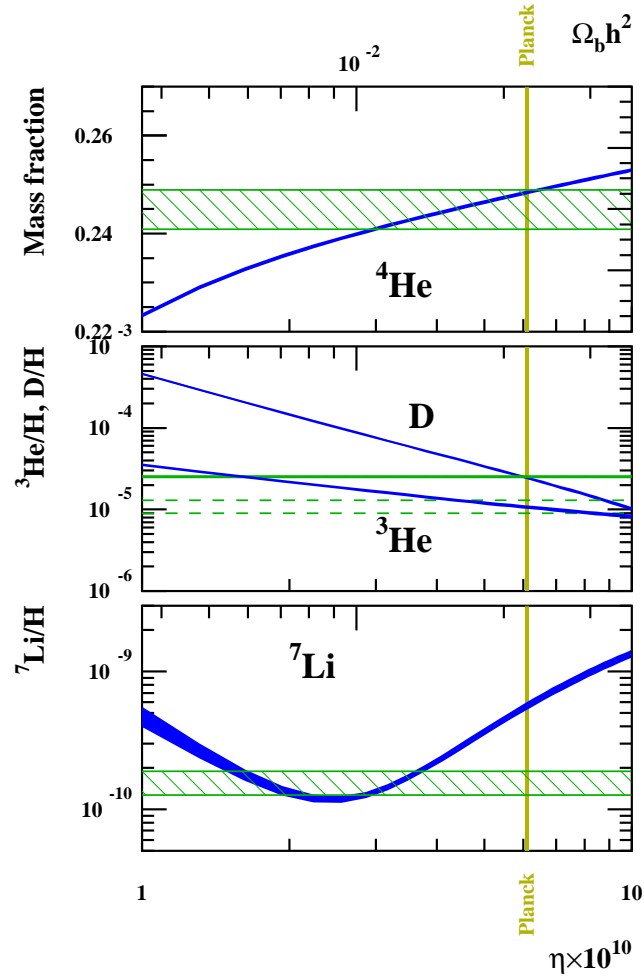


Fig. 5. Abundances of  ${}^4\text{He}$  (mass fraction), D,  ${}^3\text{He}$  and  ${}^7\text{Li}$  (by number relative to H) as a function of the baryon over photon ratio  $\eta$  or  $\Omega_b \cdot h^2$ . (Data are from Ref. 20). The vertical stripe corresponds to the CMB baryonic density<sup>6</sup> while the horizontal hatched area represent the primordial abundances (§ 3).

observations, are in good agreement except for  ${}^7\text{Li}$ , whose calculated abundance is significantly higher<sup>11,42,43</sup> (a factor of  $\approx 3.5$ ) than the primordial abundance de-

Table 1. Yields at CMB baryonic density.

	Ref. 11	This work <sup>20</sup>	Observations
<sup>4</sup> He	0.2482±0.0003	0.2484±0.0002	0.2449±0.0040 <sup>21</sup>
D/H (×10 <sup>-5</sup> )	2.64 <sup>+0.08</sup> <sub>-0.07</sub>	2.45±0.05	2.53±0.04 <sup>19</sup>
<sup>3</sup> He/H (×10 <sup>-5</sup> )	1.05±0.03	1.07±0.03	(0.9–1.3) <sup>22</sup>
<sup>7</sup> Li/H (×10 <sup>-10</sup> )	4.94 <sup>+0.40</sup> <sub>-0.38</sub>	5.61±0.26	1.58±0.31 <sup>13</sup>

duced from observations. The origin of this discrepancy between CMB+BBN and spectroscopic observations remains an open question (§ 6).

Besides those four *light elements* heavier isotopes are produced in minute amounts:<sup>32</sup> <sup>9</sup>Be/H≈1×10<sup>-18</sup>, <sup>10</sup>B/H≈3×10<sup>-21</sup>, and <sup>11</sup>B/H≈3×10<sup>-16</sup>. A special mention should be made for <sup>6</sup>Li, for which the possible existence of a plateau, in the <sup>6</sup>Li/H=10<sup>-12</sup> to 10<sup>-11</sup> range (well above the BBN yield of 1.3×10<sup>-14</sup>),<sup>44</sup> had been suggested<sup>45</sup> but has not been confirmed by subsequent observations.<sup>46</sup> The CNO standard big bang nucleosynthesis production is found to be CNO/H (0.96<sup>+1.89</sup><sub>-0.47</sub>)×10<sup>-15</sup> (too low to have an impact on Population III stellar evolution).<sup>11</sup>

## 6. The lithium problem

There are many tentative solutions to this problem (nuclear, observational, stellar, cosmological,...),<sup>47,48</sup> but none has provided yet a fully satisfactory solution. The derivation of the lithium abundance in halo stars with the high precision needed is difficult and requires a fine knowledge of the physics of stellar atmosphere (effective temperature scale, population of different ionization states, non Local Thermodynamic Equilibrium effects and 1D/3D model atmospheres). There is no lack of phenomena to modify the surface abundance of lithium: nuclear burning, rotational induced mixing, atomic diffusion, turbulent mixing, mass loss,... However, the flatness of the plateau over three decades in metallicity and the relatively small dispersion of data represent a real challenge to stellar modeling.<sup>d</sup> One also notes that between the BBN epoch and the birth of the now observed halo stars, ≈1 Gyr has passed. Primordial abundances could have been altered during this period.

### 6.1. No nuclear physics solution

Before invoking non-standard solutions to this problem nuclear solutions have been investigated. At the baryonic density deduced from CMB observations, <sup>7</sup>Li is produced indirectly by <sup>3</sup>He(α,γ)<sup>7</sup>Be, that will, much later decay to <sup>7</sup>Li while it is destroyed by <sup>7</sup>Be(n,p)<sup>7</sup>Li(p,α)<sup>4</sup>He. The <sup>3</sup>He(α,γ)<sup>7</sup>Be cross section has long been

<sup>d</sup>A recent work<sup>49</sup> suggested that pre-main sequence depletion, regulated by photo-evaporation could achieve this goal.

a subject of debate because of systematic differences that were found according to the experimental technique. This is now settled<sup>33–35</sup> and the associated uncertainty ( $\sim 5\%$ ) is very small compared to the discrepancy. To solve this problem, within conventional nuclear physics, one has to search for other reactions that could lead to  ${}^7\text{Li}+{}^7\text{Be}$  increased destruction. The  ${}^7\text{Be}(\text{d,p})2\alpha$  reaction (Fig. 3) was a prime candidate<sup>50</sup> but subsequent experiments and analyses ruled out this possibility (Kirsebom & Davids<sup>51</sup> and references therein). Extending this search, recent works<sup>52</sup> suggested the possibility of overlooked resonances in nuclear reactions involving  ${}^7\text{Be}$ , the most promising candidate was found to be in the  ${}^7\text{Be}+{}^3\text{He}\rightarrow{}^{10}\text{C}$  channel. However, in a recent experiment the upper limits for the presence of new levels in  ${}^{10}\text{C}$  (and  ${}^{11}\text{C}$ ) were found to be too low to have an impact on  ${}^7\text{Li}$  production.<sup>53</sup> The natural way of  ${}^7\text{Be}$  destruction in BBN occurs through the  ${}^7\text{Be}(\text{n,p}){}^7\text{Li}(\text{p},\alpha){}^4\text{He}$  channel which is limited by the scarcity of neutrons. Hence, since a supplementary reaction, overlooked in previous studies, seems now to be excluded by experiments,<sup>53</sup> a peculiar attention should be paid to an enhanced neutron abundance.

## 6.2. *Non standard neutron injection during BBN*

It was recognized,<sup>54,55</sup> that extra neutron injection would increase  ${}^7\text{Be}$  destruction by  ${}^7\text{Be}(\text{n,p}){}^7\text{Li}(\text{p},\alpha){}^4\text{He}$ , but at the expense of a rise in the abundance of D/H. Given the new tight constraints on D/H observations (§ 3), one may question if the neutron injection mechanism is still a valid agent for reducing the cosmological abundance of lithium. Extending the BBN network to  $\approx 400$  reactions has not lead to the identification of any overlooked conventional neutron source,<sup>32</sup> i.e. an extra neutron producing reaction. Hence, one has to investigate non standard neutron sources that can be:

- (1) *Particle decay.* This class of models assume the existence of a hypothetical particle  $X$  that can decay and produce neutron, i.e.  $X \rightarrow \text{n} + \dots$
- (2) *Particle annihilation.* These models assume  $X + X \rightarrow \text{n} + \dots$  pair annihilation.
- (3) *Resonant particle annihilation.* A narrow resonance in the annihilation cross section is present at some energy.
- (4)  *$n-n'$  oscillation.* This model<sup>56</sup> assumes that there is a mirror world from which *mirror-neutrons* can oscillate into our world. The microphysics is considered to be identical in the two sectors, but the temperatures and baryonic densities are different in the two sectors.<sup>56</sup>

Figure 6 is a summary of the results<sup>57</sup> of BBN calculations within the framework of models 1–4, while varying the relevant parameters. Each dot correspond to a set of parameters and different colors correspond to the different models. It appears that the  ${}^7\text{Be}$  destruction by the injection of extra neutrons is accompanied by the deuterium over-production, i.e. that lithium and deuterium abundances are anti-correlated as seen, e.g., in an instantaneous neutron injection model (Fig. 4 in Kusakabe et al.<sup>58</sup>) or in a massive gravitino decay model (Fig. 1 in Olive et al.<sup>59</sup>).

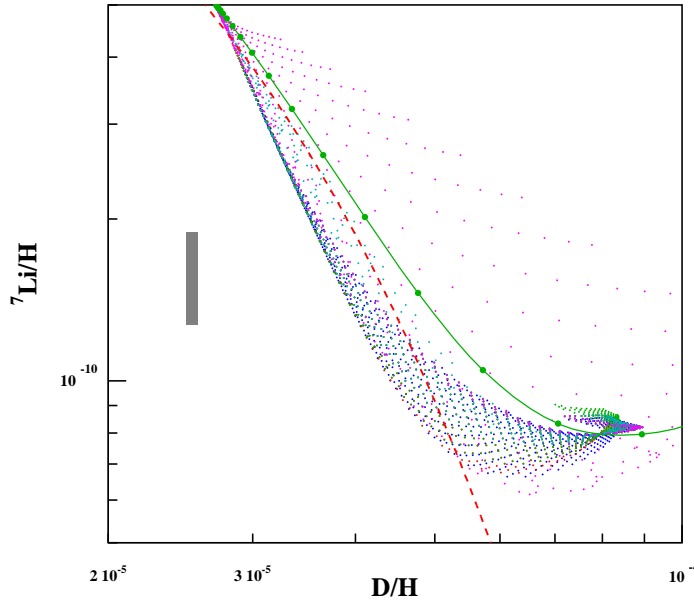


Fig. 6. Each dot is the prediction of a model<sup>57</sup> in the space  $(D/H, {}^7\text{Li}/H)$ . The rectangle corresponds to the  $D/H$  observational limits of Ref. 19 together with those from Ref. 13 for lithium. The blue, red and green dots correspond to  $n$ - $n'$  oscillation models the light blue dots correspond to resonant annihilation models and the pink dots to particle decay models. The green curve with filled circles corresponds to the non-resonant annihilation model. The dashed line is a qualitative explanation of this anti-correlation.<sup>20</sup> This demonstrates that no model can be in agreement with both lithium-7 and deuterium

The reason for this anti-correlation is that besides  ${}^7\text{Be}$  destruction by  ${}^7\text{Be}(n,p){}^7\text{Li}$ , late time neutron injection, *unavoidably* generate extra deuterium by the  ${}^1\text{H}(n,\gamma)\text{D}$  reaction.<sup>20,58</sup> Neglecting all other reactions, at the relevant temperature when  ${}^7\text{Be}$  is formed, one obtains<sup>20</sup> the dashed curve in Fig. 6. The lower limit for lithium abundance appears at  $\text{Li}/H \approx 6 \times 10^{-11}$  (Fig. 6). It comes from the enhanced  ${}^3\text{H}$  production [by  ${}^3\text{He}(n,p){}^3\text{H}$ ] that feeds the  ${}^3\text{H}(\alpha,\gamma){}^7\text{Li}$  branch (“Low  $\Omega_B$ ” on Fig. 3) while  ${}^7\text{Li}$  may not be efficiently destroyed anymore by  ${}^7\text{Li}(p,\alpha){}^4\text{He}$ , because of the lower temperature.

## 7. Deuterium cosmic evolution

Starting from our new BBN  $D/H$  value at redshift of  $z \approx 10^8$ , it is interesting to follow the cosmic deuterium evolution. This isotope is a good tracer of stellar formation since it can only be destroyed from the BBN epoch due to its fragility

(burnt at  $T > 10^5$  K, deuterium is destroyed throughout the cosmic evolution).

The observational constraints on D/H evolution with redshift, besides the cosmological data from damped Lyman- $\alpha$  (DLA) systems at  $z \approx 2 - 3$ , already discussed in Section 3, come from the local D/H observations at present day ( $z = 0$ ). Prodanovic et al.<sup>65</sup> estimate the interstellar medium (ISM) deuterium abundance to be  $D/H > (2.0 \pm 0.1) \times 10^{-5}$ , leading to an astration factor  $f_D$  (which is the ratio,  $D_{\text{BBN}}/D_{\text{present}}$ ), of  $f_D < 1.26 \pm 0.1$ . Linsky et al.<sup>64</sup> study reveals a very wide range of observed D/H ratio in the local galactic disk and give as the most representative value  $D/H > (2.31 \pm 0.24) \times 10^{-5}$ , leading to an astration factor,  $f_D$ , of less than 1.1.

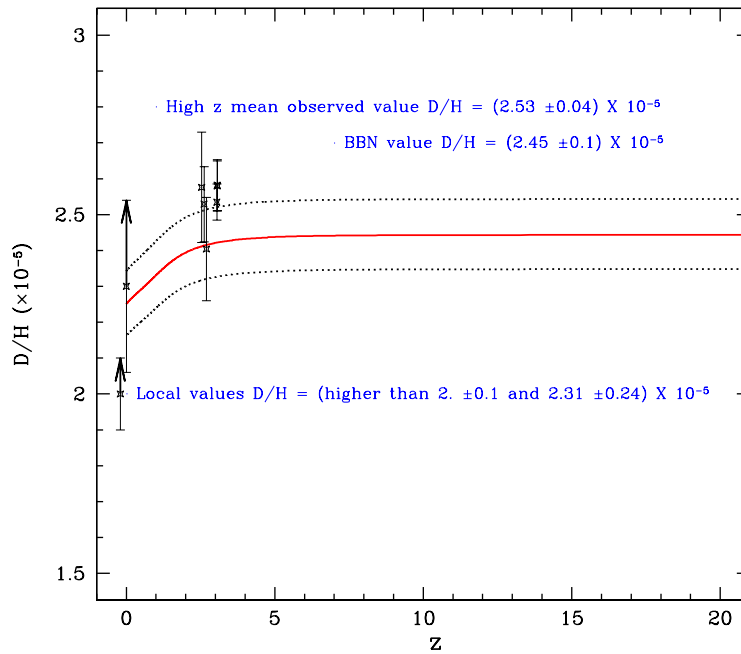


Fig. 7. Cosmic D evolution as a function of redshift. The red solid curve corresponds to the evolution of D/H using our mean BBN value whereas the black dotted curves correspond to the higher and lower  $2\sigma$  limits. High  $z$  DLAs observations come from Cooke et al.<sup>19</sup> whereas local observations come from Linsky et al.<sup>64</sup> and Prodanovic et al.<sup>65</sup>

Cosmic chemical evolution depends on a stellar initial mass function (IMF) and a star formation rate (SFR). Their convolution is measurable through the total observed luminosity density. Recently, improvements have been made in our

understanding of the global star formation history, particularly at high redshift.

SFR evolution with redshift is constrained by many observations. Specifically, recent data from high redshift galaxy observations (the Hubble Ultra Deep Field) have significantly extended the range of redshifts for its determination, from  $z = 4$  up to 10.<sup>66,67</sup> It is a key ingredient to all evolution models. For a comprehensive discussion of these observational advances, see Bouwens et al.<sup>68</sup>

In this context we consider the cosmic evolution of D/H in a cosmological way in the light of the new, somewhat low, D primordial value derived here. Indeed, we follow its cosmic evolution using a model developed in Refs. 60, 61, 62, based on a hierarchical model for structure formation (Press and Schechter formalism<sup>63</sup>), and we determine the rate at which structures accrete mass. The model follows the evolution of the amount of baryons in stars, in structures (ISM) and in the intergalactic medium (IGM). The model includes also a description of mass exchanges between the IGM and ISM (structure formation, galactic outflows), and between the ISM and the stellar component (star formation, stellar winds and supernova explosions).

Once the cosmic SFR is specified, several quantities are obtained as a function of redshift, namely the abundances of chemical elements, SN rates, reionization of the universe, and more specifically deuterium. Deuterium destruction is governed by low mass stars (since the gas is essentially trapped in these stars and is released only, long after, at low redshift) whereas metallicity production (elements others than H and He) is governed by high mass stars which reject enriched matter at high redshift. A weak destruction of D is consequently not incompatible with a significant formation of heavy elements.

We consider here the results of the best model described in Ref. 62, including a standard mode of Pop II/I stars formation between 0.1 and 100 solar masses. The IMF slope is set to the Salpeter value, i.e.  $x = 1.35$ .<sup>69</sup> Figure 7 shows the evolution of D/H as a function of redshift starting from our  $2\sigma$  BBN limits. Black dotted curves correspond to the present BBN limits, whereas the red solid line corresponds to the mean. The resulting astration factor is  $f_D = 1.1$ . This cosmic evolution is in overall agreement with the observed values, implying that the mean abundance of deuterium has only been reduced by a factor of 1.1 to 1.25 (see Ref. 20) since its formation. Note however that a tension exists between the BBN D/H value and the high  $z$  measurements leaving clearly little room for a high astration factor.

## 8. Statistical methods in (big bang) nucleosynthesis

Improved techniques have been developed in nucleosynthesis calculations to evaluate uncertainties on the final results and to identify the main sources of these uncertainties. It is of special interest for BBN because of the commensurate uncertainties on calculated and observed abundances, while the lithium problem (§ 6) remains unsolved.

At first, simple sensitivity studies<sup>30,37</sup> (i.e. varying one reaction rate at a time)

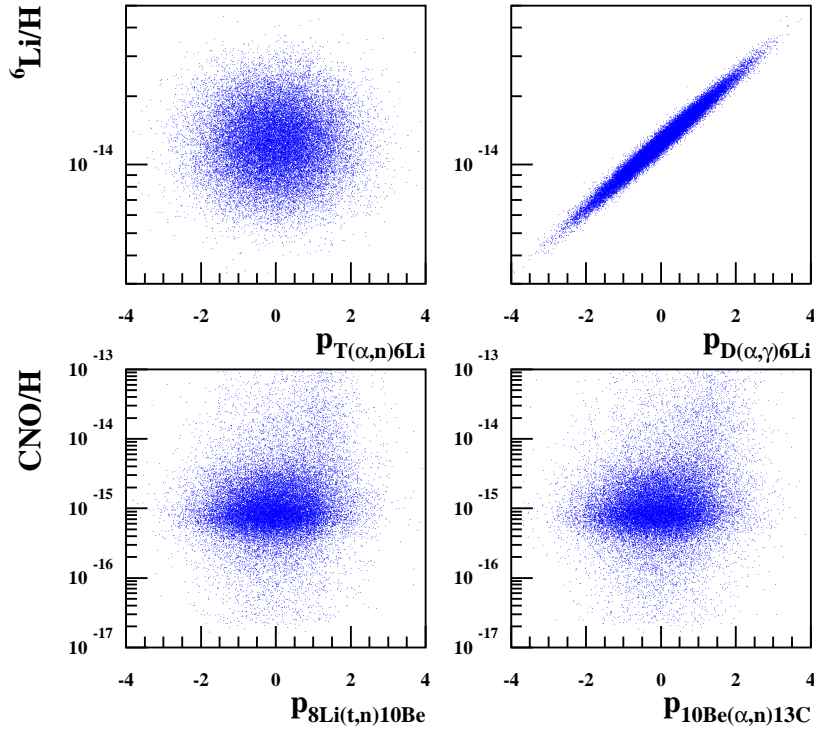


Fig. 8. Top panels: scatter plots of  ${}^6\text{Li}$  yields versus random enhancement factors ( $p_k$ ) applied to reaction rates in the context of BBN, showing no  $[\text{T}(\alpha,\text{n}){}^6\text{Li}]$  or very strong  $[\text{D}(\alpha,\gamma){}^6\text{Li}]$  correlation with  ${}^6\text{Li}$ . Bottom panels: enhancement plots of CNO/H yields versus random enhancement factors ( $p_k$ ) applied to reaction rates showing weak correlation with respectively  ${}^8\text{Li}(\text{t},\text{n}){}^{10}\text{Be}$  and  ${}^{10}\text{Be}(\alpha,\text{n}){}^{13}\text{C}$  reactions (data are from Ref. 11).

have identified the most important BBN reactions for the production of the light elements. Unexpected effect can be found this way like the high sensitivity of the  ${}^7\text{Li}$  yield to the  ${}^1\text{H}(\text{n},\gamma){}^2\text{H}$  rate or that an increase of the  ${}^7\text{Li}(\text{d},\text{n}){}^4\text{He}$  reaction rate reduces the CNO abundance,<sup>32</sup> even though the D and  ${}^7\text{Li}$  *final abundances are left unchanged*. However, the greatest improvement comes from the Monte Carlo technique, now widely used in nucleosynthesis calculations.<sup>70</sup> Ideally reaction rate uncertainties are known, together with the associated probability density functions (p.d.f.). As described in Longland *et al.*,<sup>71</sup> this can be obtained by Monte Carlo calculations taking into account uncertainties and p.d.f. of experimentally (or theoretically) determined quantities that enter into the rate calculations. Reaction rate p.d.f. can usually be represented by a log-normal distribution whose parameters



are tabulated as a function of temperature.<sup>71</sup> These reaction rate p.d.f. can then be used in nucleosynthesis Monte Carlo calculations where all reaction rates are sampled independently. From the resulting histograms of calculated abundances, the median and 68% confidence interval is obtained from the 0.5, 0.16 and 0.84 quantiles. This is how the confidence intervals quoted here are obtained.

Namely the reaction rates  $N_A\langle\sigma v\rangle_k$ , (with  $k$  being the index of the reaction), are assumed to follow a lognormal distribution:

$$N_A\langle\sigma v\rangle_k = \exp(\mu_k(T) + p_k\sigma_k(T)) \quad (8)$$

where  $p_k$  is sampled according to a *normal* distribution of mean 0 and variance 1 (Eq. (22) of Ref. 72). The  $\mu_k$  and  $\sigma_k$  determine the location of the distribution and its width, which are tabulated as a function of  $T$ . First, by taking the quantiles of the Monte Carlo calculated distributions of final isotopic abundances one obtains, not only their median values but also the associated confidence interval. Second, the (Pearson's) correlation coefficient between isotopic abundance  $y_j$  and reaction rate random enhancement factors ( $p_k$  in Eq. 8) can be calculated. Figure 8, in the top panels, shows simple cases where there is no or a very strong correlation between a yield and two reaction rates. A simple sensitivity study would have been sufficient here, but the bottom panels displays some weak correlation between the CNO production and two reaction rates. These were not recognized in a study, changing each of these reaction rate, *one at a time*, by factors up to 1000.<sup>32</sup> This explain that in a Monte Carlo BBN calculation of CNO abundance, in the resulting distribution (Figure 4 of Ref. 11), for  $\approx 2\%$  of the cases,  $\text{CNO}/\text{H} > 10^{-13}$ , a value that may affect first stars throughout their evolution (Pop III stars). A *combination* of higher rates together with lower rates for a few reactions around  $^{10}\text{Be}$  (Fig. 3) lead to this effect.<sup>11</sup> This was not seen without the use of Monte Carlo and correlation analyses; a combined technique that can be extended to other sites of nucleosynthesis.<sup>73</sup>

## 9. Conclusion

The agreement between BBN predictions and observations is quite satisfactory except for lithium. Many studies have been devoted to the resolution of this lithium problem and many possible “solutions”, none fully satisfactory, have been proposed. For a detailed analysis see<sup>47</sup> and the various contributions to the meeting “Lithium in the cosmos”.<sup>48</sup> In particular nuclear physics solutions, leading to an increased  $^7\text{Be}$  destruction, have been experimentally investigated, and can now be excluded.<sup>53</sup> Now that the D/H primordial abundance is expected to be known with an improved precision,<sup>19</sup> nuclear cross sections of all reactions leading to D destruction should be determined with an equal precision.<sup>20,36</sup>

Nevertheless, primordial nucleosynthesis remains a invaluable tool for probing the physics of the early universe. When we look back in time, it is the ultimate process for which we *a priori* know all the physics involved: departure from its predictions provide hints for new physics or astrophysics. Hence, there are two

motivations to extend BBN beyond the standard model: use it to probe the early universe and to test fundamental physics<sup>7,8</sup> on the one hand, and find a solution to the lithium problem<sup>47</sup> on the other hand.

Gravity that could differ from its general relativistic description, affecting the rate of expansion of the universe (see Ref. 74 for a review), or the variation of the fundamental constants (see Ref. 75 for a review), can be constrained by BBN.<sup>76,77</sup> The decay of a massive particle during or after BBN could affect the light element abundances and potentially lower the  ${}^7\text{Li}$  abundance (see e.g. Ref. 78 and references therein). This effect could also be obtained with negatively charged relic particles, like the supersymmetric partner of the tau lepton, that could form bound states with nuclei, lowering the Coulomb barrier and hence leading to the catalysis of nuclear reactions (see e.g. Ref. 79 and references therein). Non-standard solutions to the lithium problem include photon cooling,<sup>80</sup> possibly combining particle decay and magnetic fields.<sup>81</sup>

Last but not least, we stress here the importance of sensitivity studies in nuclear astrophysics: even in the simpler context of BBN without the complexity (e.g. mixing) of stellar nucleosynthesis, it would have been very unlikely to predict the influence of the  ${}^1\text{H}(n,\gamma){}^2\text{H}$  reaction on  ${}^7\text{Li}$  nor of the  ${}^7\text{Li}(d,n){}^4\text{He}$  reaction on CNO, before these systematic investigations.

## Acknowledgements

We are indebted to our collaborators on these topics: Pierre Descouvemont, Faïrouz Hammache, Stéphane Goriely, Christian Iliadis, Richard Longland, Keith Olive, Patrick Petitjean, Maxim Pospelov and Jean-Philippe Uzan. This work made in the ILP LABEX (under reference ANR-10-LABX-63) was supported by French state funds managed by the ANR within the Investissements d’Avenir programme under reference ANR-11-IDEX-0004-02 and by the ANR VACOUL, ANR-10-BLAN-0510.

## References

1. R.V. Wagoner, *Astrophys. J.* **179** (1973) 343.
2. J. Yang, D. Schramm, G. Steigman and R. T. Rood, *Astrophys. J.* **227** (1979) 697.
3. The ALEPH Collaboration (S. Schael et al.) and The DELPHI Collaboration (J. Abdallah et al.) and the L3 Collaboration (M. Acciarri et al.) and The OPAL collaboration (G. Abbiendi et al.) and The SLD Collaboration (Kenji Abe et al.) and the LEP Electroweak Working Group and the SLD Electroweak and Heavy Flavour Groups, *Phys. Rep.* **427** (2006) 257.
4. G. Hinshaw, D. Larson, E. Komatsu et al., *Astrophys. J. S.* **208** (2013) 19.
5. *Planck* Collaboration XVI, P.A.R. Ade, N. Aghanim, C. Armitage-Caplan, M. Arnaud, M. Ashdown et al., *Astron. Astrophys.* **571** (2014) A16.
6. *Planck* Collaboration XIII, P.A.R. Ade, N. Aghanim, M. Arnaud, M. Ashdown, J. Aumont et al., *Astron. Astrophys.* **594** (2016) A13.
7. F. Iocco, G. Mangano, G. Miele, O. Pisanti and P. D. Serpico, *Phys. Rev.* **472** (2009) 176.

8. M. Pospelov and J. Pradler, *Annual Review of Nuclear and Particle Science* **60** (2010) 539.
9. S. Weinberg, *Cosmology*, Oxford University Press, 2008, ISBN 978-0-19-852682-7.
10. M. Fukugita and P.J.E. Peebles, *Astrophys. J.* **616** (2004) 643.
11. A. Coc, J.-P. Uzan, and E. Vangioni *J. Cosmology Astropart. Phys.* **10** (2014) 050 [arXiv:1403.6694 \[astro-ph.CO\]](#).
12. F. Spite and M. Spite, *Astron. Astrophys.*, **115** (1982) 357.
13. L. Sbordone, P. Bonifacio, E. Caffau et al., *Astron. Astrophys.*, **522** (2010) 26.
14. J.C. Howk, N. Lehner, B.D. Fields and G.J. Mathews, *Nature* **489** (2012) 121.
15. A. Tajitsu, K. Sadakane, H. Naito, A. Arai and W. Aoki, *Nature* **518** (2015) 381.
16. L. Izzo, M. Della Valle, E. Mason, F. Matteucci, D. Romano et al., *Astrophys. J.* **808** (2015) L14.
17. M. Hernanz, J. José, A. Coc and J. Isern, *Astrophys. J.* **465** (1996) L27.
18. M. Pettini and M. Cooke, *Mon. Not. R. Astron. Soc.* **425** (2012) 2477.
19. R. Cooke, M. Pettini, R.A. Jorgenson, M.T. Murphy and C.C. Steidel, *Astrophys. J.* **781** (2014) 31.
20. A. Coc, P. Petitjean, J.-P. Uzan, E. Vangioni, P. Descouvemont, C. Iliadis and R. Longland, *Phys. Rev. D* **92** (2015) 123526 [arXiv:1511.03843 \[astro-ph.CO\]](#).
21. E. Aver, K.A. Olive and E.D. Skillman, *J. Cosmology Astropart. Phys.* **07** (2015) 011 [arXiv:1503.08146v1 \[astro-ph.CO\]](#)
22. T. Bania, R. Rood and D. Balser, *Nature* **415** (2002) 54.
23. D. Dicus, E. Kolb, A. Gleeson, E. Sudarshan, V. Teplitz and M. Turner, *Phys. Rev. D* **26** (1982) 2694.
24. K.A. Olive et al. (Particle Data Group), *Chin. Phys. C* **38** (2014) 090001 URL: <http://pdg.lbl.gov>
25. F. Wietfeldt and G. Greene, *Rev. Mod. Phys.* **83** (2011) 1173.
26. A.R. Young, S. Clayton, B.W. Filippone, P. Geltenbort, T.M. Ito, C.-Y. Liu, M. Makela, C.L. Morris, B. Plaster, A. Saunders, S.J. Seestrom and R.B. Vogelaar, *J. Phys. G: Nucl. Part. Phys.* **41** (2014) 114007.
27. G. J. Mathews, T. Kajino and T. Shima *Phys. Rev. D* **71** (2005) 021302(R).
28. S. Ando, R.H. Cyburt, S.W. Hong and C.H. Hyun, *Phys. Rev. C* **74** (2006) 025809.
29. P. Descouvemont, A. Adahchour, C. Angulo, A. Coc and E. Vangioni-Flam, *At. Data Nucl. Data Tables* **88** (2004) 203.
30. R.H. Cyburt, *Phys. Rev. D* **70** (2004) 023505.
31. P.D. Serpico, S. Esposito, F. Iocco, G. Mangano, G. Miele and O. Pisanti, *J. Cosmology Astropart. Phys.* **12** (2004) 010.
32. A. Coc., S. Goriely, Y., Xu, M. Saimpert and E. Vangioni, *Astrophys. J.* **744** (2012) 158.
33. A. Di Leva, L. Gialanella, R. Kunz et al., *Phys. Rev. Lett.* **102** (2009) 232502.
34. R.H. Cyburt and B. Davids, *Phys. Rev. C* **78** (2008) 064614.
35. R. J. deBoer, J. Görres, K. Smith, E. Uberseder, M. Wiescher, A. Kontos, G. Imbriani, A. Di Leva and F. Strieder, *Phys. Rev. C* **90** (2014) 035804.
36. E. Di Valentino, C. Gustavino, J. Lesgourgues, G. Mangano, A. Melchiorri, G. Miele and O. Pisanti, *Phys. Rev. D* **90** (2014) 023543.
37. A. Coc and E. Vangioni, *Journal of Physics Conference Series*, **202** (2010) 012001.
38. D.S. Leonard, H.J. Karwowski, C.R. Brune, B.M. Fisher and E.J. Ludwig, *Phys. Rev. C* **73** (2006) 045801.
39. K. Arai, S. Aoyama, Y. Suzuki, P. Descouvemont and D. Baye, *Phys. Rev. Lett.* **107** (2011) 132502.
40. L.E. Marcucci, M. Viviani, R. Schiavilla, A. Kievsky and S. Rosati, *Phys. Rev. C* **72**

20 *A. Coc and E. Vangioni*

- (2005) 014001; Laura Elisa Marcucci *priv. comm.*.
41. S.Q. Hou, J.J. He, S. Kubono and Y.S. Chen, *Phys. Rev. C* **91** (2015) 055802 [arXiv:1502.03961 \[astro-ph.CO\]](#).
  42. R.H. Cyburt, B.D. Fields and K.A. Olive, *J. Cosmology Astropart. Phys.* **11** (2008) 012.
  43. R.H. Cyburt, B.D. Fields, K.A. Olive and T.-H. Yeh, *Rev. Mod. Phys.* **88** (2016) 015004 [arXiv:1505.01076 \[astro-ph.CO\]](#).
  44. F. Hammache, M. Heil, S. Typel et al. *Phys. Rev. C* **82** (2010) 065803 .
  45. M. Asplund, D. Lambert, P.E. F. Nissen, F. Primas and V. Smith, *Astrophys. J.*, **644** (2006) 229.
  46. K. Lind, J. Melendez, M. Asplund, R. Collet and Z. Magic, *Astron. Astrophys.* **554** (2013) A96.
  47. B. Fields, *Annu. Rev. Nucl. Part. Sci.* **61** (2011) 47.
  48. M. Spite, F. Spite and P. Bonifacio *Mem. S.A.It. Suppl.* **22** (2012) 9.
  49. X. Fu, A. Bressan, P. Molaro and P. Marigo, *Mon. Not. R. Astron. Soc.* **452**, (2015) 3256 [arXiv:1506.05993v1 \[astro-ph.SR\]](#).
  50. A. Coc, A., E. Vangioni-Flam, P. Descouvemont, A. Adahchour and C. Angulo, *Astrophys. J.* **600** (2004) 544.
  51. O.S. Kirsebom and B. Davids, *Phys. Rev. C* **84** (2011) 058801.
  52. N. Chakraborty, B.D. Fields and K.A. Olive, *Phys. Rev. D* **83** (2011) 063006.
  53. F. Hammache, A. Coc, N. de Séréville et al., *Phys. Rev. C* **88** (2013) 062802(R) [arXiv:1312.0894 \[nucl-ex\]](#).
  54. M. H. Reno and D. Seckel, *Phys. Rev. D* **37** (1988) 3441.
  55. K. Jedamzik, *Phys. Rev. D* **70** (2004) 063524.
  56. Z. Berezhiani, D. Comelli and F.L. Villante, *Phys. Lett. B* **503** (2001) 362.
  57. A. Coc, M. Pospelov, J.-Ph. Uzan and E. Vangioni *Phys. Rev. D* **90** (2014) 085018 [arXiv:1405.1718 \[astro-ph\]](#).
  58. M. Kusakabe, M.-K. Cheoun and K. S. Kim, *Phys. Rev. D* **90** (2014) 045009.
  59. K. Olive, P. Petitjean, E. Vangioni and J. Silk, *Mon. Not. R. Astron. Soc.*, **426** (2012) 1427.
  60. F. Daigne, K.A. Olive, J. Silk, F. Stoehr and E. Vangioni, *Astrophys. J.* **647** (2006) 773.
  61. E. Rollinde, E. Vangioni, D. Maurin, K.A. Olive, F. Daigne, J. Silk, and F.H. Vincent, *Mon. Not. R. Astron. Soc.* **398** (2009) 1782.
  62. E. Vangioni, K.A. Olive, T. Prestegard, J. Silk, P. Petitjean and V. Mandic, *Mon. Not. R. Astron. Soc.* **447** (2014) 2575 [arXiv:1409.2462 \[astro-ph.GA\]](#).
  63. W.H. Press & P. Schechter *Astrophys. J.* **187** (1974) 425.
  64. J.L. Linsky, B.T. Draine, H.W. Moos, et al., *Astrophys. J.* **647** (2006) 1106.
  65. T. Prodanović, G. Steigman and B. D. Fields, *Mon. Not. R. Astron. Soc.* **406** (2010) 1108.
  66. P.A. Oesch, R.J. Bouwens, and G.D. Illingworth, et al., *Astrophys. J.* **786** (2014) 108.
  67. R. J. Bouwens, L. Bradley, A. Zitrin, et al., *Astrophys. J.* **795** (2014) 126.
  68. R. J. Bouwens, R.J. Illingworth, G.D. Oesch, et al., *Astrophys. J.* **803** (2015) 34.
  69. E.E. Salpeter, *Astrophys. J.* **121**, 161 (1955).
  70. C. Iliadis, R. Longland, A. Coc, F.X. Timmes & A. E. Champagne, *J. Phys. G: Nucl. Part. Phys.*, **42** (2015) 034007 [arXiv:1409.5541 \[nucl-ex\]](#).
  71. R. Longland, C. Iliadis, A. E. Champagne et al., *Nucl. Phys. A* **841** (2010) 1.
  72. A.L. Sallaska, C. Iliadis, A.E. Champagne S. Goriely, S. Starrfield, F. X. Timmes, *Astrophys. J. S.* **207** (2013) 18 [arXiv:1304.7811 \[astro-ph.SR\]](#), <http://starlib.physics.unc.edu/index.html>.

73. A. Parikh, J. José, F. Moreno, C. Iliadis, *Astrophys. J. S.* **178** (2008) 110.
74. J.-P. Uzan, *General Relativity and Gravitation*, **42** (2010) 2219.
75. J.-P. Uzan, *Living Reviews in Relativity*, **14** (2011) 2.
76. A. Coc, K. Olive, J.-P. Uzan and E. Vangioni *Phys. Rev. D* **79** (2009) 103512.
77. A. Coc, P. Descouvemont, K. Olive, J.-P. Uzan and E. Vangioni, *Phys. Rev. D* **86** (2012) 043529.
78. R. H. Cyburt, J. Ellis, B. D. Fields, F. Luo, K. A. Olive and V. C. Spanos *J. Cosmology Astropart. Phys.* **05** (2013) 014.
79. M. Kusakabe, K. S. Kim, M.-K. Cheoun, T. Kajino and Y. Kino, *Phys. Rev. D* **88** (2013) 063514.
80. O. Erken, P. Sikivie, H. Tam and Q. Yang *Phys. Rev. D* **85** (2012) 063520.
81. D. G. Yamazaki, M. Kusakabe, T. Kajino, G.J. Mathews and M.K. Cheoun, *Phys. Rev. D* **90** (2014) 023001.